Silicon and silicon–copper composite nanorods for anodes of Li-ion rechargeable batteries

Ming Au [a,*], Yuping He [b], Yiping Zhao [b], Hessam Ghassemi [c], Reza Shahbazian Yassar [c], Brenda Garcia-Diaz [a], Thad Adams [a]

[a] Savannah River National Laboratory, Aiken, SC, USA
[b] Department of Physics and Astronomy, and Nanoscale Science and Engineering Center, University of Georgia, Athens, GA 30602, USA
[c] Michigan Technological University, Houghton, MI, USA

ARTICLE INFO

ABSTRACT

We investigate the anode performance of Si-based nanorods by tuning its composition using an oblique (co)deposition technique. Our results show that pure Si nanorods have a higher initial anodic capacity of 1500 mAh g^{-1}, but the capacity diminishes after 50 cycles due to the morphological change and pulverization. By introducing approximately 70 at.% Cu into Si nanorods, the Si–Cu composite nanorods demonstrate 500 mAh g^{-1} of capacity sustainable in 100 cycles, which is attributed to the flexibility and improved toughness of Si–Cu composite nanorods.

Currently, the plug-in hybrid and electric vehicles are promoted for leading the way of the migration from fossil fuel propulsion to electrification of the transportation. Lacking of the advanced batteries with high energy densities and low cost is one of several technical challenges for such a transition. A number of metals and metal oxides have been investigated as the candidates for the high capacity anodes for lithium ion batteries [1–11]. However, the large volume expansion (300–400%) during metal-lithium alloying or oxide-lithium conversion causes pulverization of anode materials and therefore results in rapid decrease in the capacity. To improve the electric conductivity and mechanical integrity of the electrodes, in general, the powdery metals or metal oxides have to be mixed with conductive additives, binders, and solvent before being pasted on current collectors. This electrode fabrication involves powder grinding, slurry blending, casting, calendaring, and baking. The process is not only complicated and costly, but also causes environment concerns. The lacking of direct contact of the active materials and the current collectors limits the power densities and requires longer charge time. Tailoring active materials into aligned nanostructures (i.e. nanorods) on current collectors provides one potential solution for above problems. The interstitial space in-between aligned nanorods could accommodate the volume changes and provide massive access sites for shuttling of Li ions resulting in low stress, pulverization resistance and long cycling life. The nanorods grown from current collectors have direct electronic contact that contributes to high powder density. In our previous study, the high capacity of aluminum nanorods is not sustainable during repeatedly charging and discharging because of the stress build-up at the interface of nanorods and substrate resulting in poor electrical conductivity and consequently peeling off from the current collector [1]. The Si nanowires synthesized by chemical vapor deposition (CVD) process demonstrated 3000 mAh g^{-1} of capacity up to 10 cycles at C/20 rate. The fabrication process uses the flammable and harmful gas, SiH$_4$, as the precursor and the anode charging process is limited to small current due to poor conductivity of pure Si. The long term performance of the Si nanowires has not reported yet [12]. Distributing strain and stress gradually along the nanorods may provide a solution for retention of initial high capacity. It is reported that the carbon–aluminum–silicon strain-graded nanorods synthesized by glancing angle deposition show longer cycling life, 350 mAh g^{-1} in 100 cycles [13]. However, the capacity of silicon was heavily discounted due to significant addition of carbon and aluminum. Since Cu has the superior conductivity and good solubility for Si, it is expected that the composite Si–Cu aligned nanorods will offer improved conductivity, mechanical flexibility, and strong binding to the Cu current collectors as anodes for sustainable long term cycling.

* Corresponding author. Tel.: +1 803 507 8547; fax: +1 803 652 8137.
E-mail address: ming.au@srnl.doe.gov (M. Au).
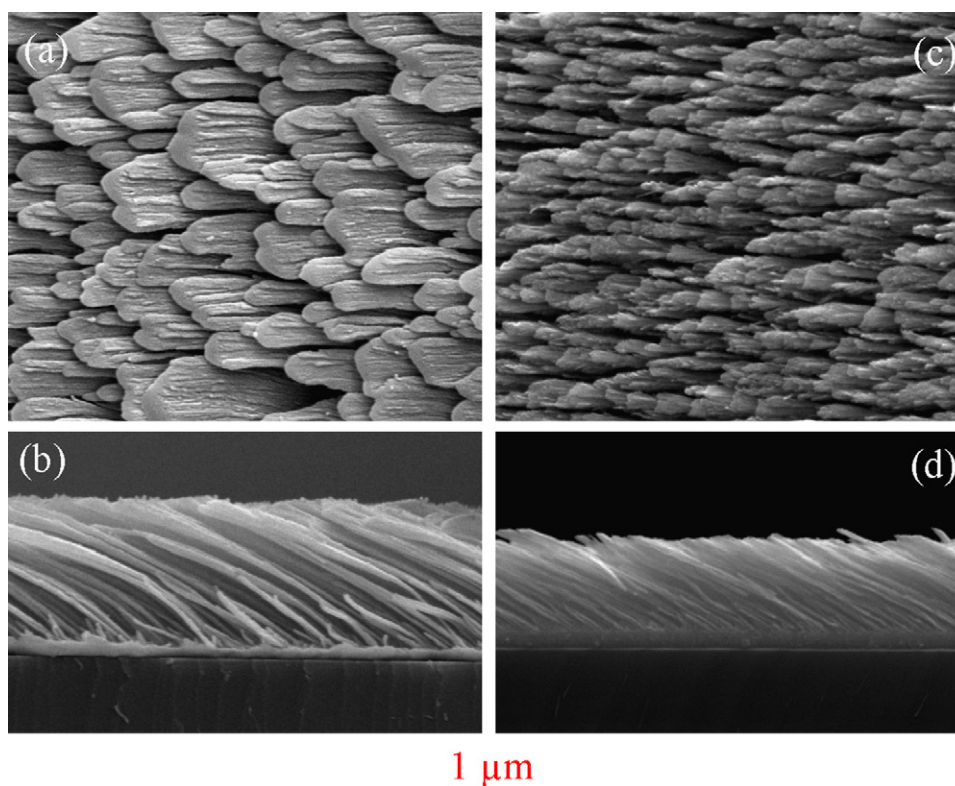
Fig. 1. SEM images: (a) top view and (b) cross view of the as-prepared Si nanorod array; (c) top view and (d) cross view of the as-prepared Si–Cu composite nanorod array.

In this work, we have fabricated aligned Si and Si–Cu composite nanorod arrays using an oblique angle (co)deposition method and compared their performance as Li^+ battery anodes. With the addition of Cu in the Si nanorods, the battery's high capacity can be sustained for multiply cycles.

1. Experimental

Both the pure Si and Si–Cu composite nanorods were fabricated by an oblique angle (co)deposition technique in a custom designed two-source electron-beam deposition system, where two quartz crystal microbalances (QCMs) were installed to monitor the near-normal deposition thickness and rate of each source independently [14–17]. During the anode nanostructure fabrication, first, a layer of 200 nm thick Cu film was coated onto the 10 mm × 30 mm glass substrates as the current collector of battery anodes at a deposition rate of $r_{Cu} = 0.2$ nm s^{-1}. Then, either pure Si or Si–Cu nanorods were deposited on the Cu film coated glass substrates at a vapor incident angle of $\alpha = 88°$ with respect to the substrate normal. The pure Si nanorods were grown at $r_{Si} = 0.4$ nm s^{-1} until QCM read 4 μm. To fabricate Si–Cu composite nanorods, both Cu and Si sources were co-evaporated at $r_{Cu} = 0.5$ nm s^{-1} and $r_{Si} = 0.4$ nm s^{-1} until QCM read 2 μm for Cu and 1.6 μm for Si. The mass of the active Si on an area of 10 mm × 30 mm is estimated to be approximately 9.3×10^{-5} g for pure Si nanorods and 3.7×10^{-5} g for the Si–Cu composite nanorods, respectively. In addition, the obtained Si–Cu composite nanorods have the atomic ratio of Cu to Si of $\gamma \approx 2$ (i.e., 70 ± 3 at.% Cu), based on energy dispersive spectroscopy (EDS) analysis.

The morphology and structure of both Si and Si–Cu nanorods were characterized by field-emission scanning electron microscopes (SEM, FEI Inspect F and Hitachi S4800), a transition electron microscope (TEM, JEOL JEM-4000FX), and a grazing angle X-ray diffractometer (XRD, PANalytical X'Pert PRO MRD) using Cu K_α radiation with the X-ray incident angle of 0.5°. To observe the morphology change during Li charge and discharge, the anodes were taken out of the battery cell during charged and discharged states and rinsed with DMC (Dimethyl Carbonate). After the anodes dried, SEM analysis was performed at different states: virgin (as-deposited samples), 50% discharged and 100% discharged in the first cycle, and 100% discharged after 100 cycles. To make TEM samples, both Si and Si–Cu nanorods were dispersed into ethanol, and then droplets of the solution were placed on the Ni grid for TEM and electron diffraction (ED) examination.

To compare their mechanical rigidness and flexibility, the individual Si and Si–Cu nanorods that were grown directly on copper
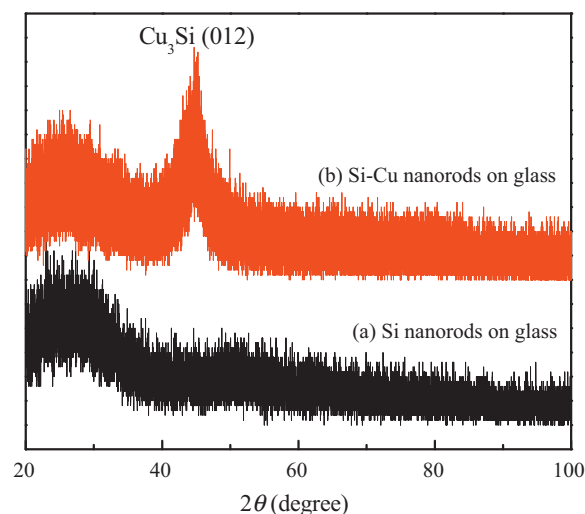
Fig. 2. XRD patterns of the as-prepared nanorods on glass substrates: (a) Si nanorods; (b) Si–Cu composite nanorods.
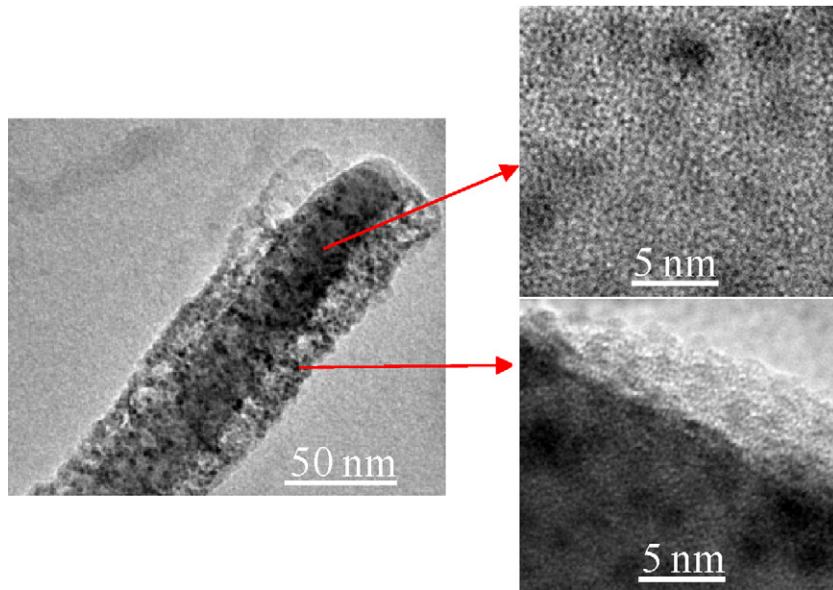
Fig. 3. TEM images of a single Si–Cu nanorod.

substrate were subjected to force measurements by a Dimension Icon atomic force microscopy (AFM). The TAP-525A probes (manufactured by Bruker Inc.) with stiffness of $\sim 200\,\mathrm{N\,m^{-1}}$ were used. The deflection sensitivity of the cantilevers was calibrated using a sapphire substrate with known elastic modulus. The measurements of force–displacement were performed on at least 8 nanorods to minimize the statistical errors.

A beaker cell of Li-ion battery was constructed in VAC (Vacuum Atmosphere Cooperation) glove box filled with argon gas. Both the Si nanorod array (or Si–Cu nanorod array) and a Li foil (Aldrich) were inserted in the cell as the anode and cathode. The 1 M $LiPF_6$ in PC/DMC (Propylene Carbonate and Dimethyl Carbonate) was purchased from Ferro and used as the electrolyte. Princeton Applied Physics' VersaSTAT-3 was used for the measurement of electrochemical properties of the anodes. The galvanic charge–discharge was carried out at $700\,\mathrm{mA\,g^{-1}}$ from 0.01 V to 3.00 V. Cyclic voltammetry (CV) was measured at $0.1\,\mathrm{mV\,s^{-1}}$ from 0.01 V to 3.00 V. The capacity was calculated based on total mass of the anode (for Si–Cu nanorod the mass includes both Si and Cu).

2. Results and discussion

2.1. Structural characterization

As shown by the SEM images in Fig. 1, both the virgin Si and Si–Cu samples consist of arrays of well-aligned and tilted nanorods; however, the addition of Cu changes the morphology of Si significantly. From the top view, the width of the nanorods close to their tips is $w_{Si} = 600 \pm 300$ nm for Si nanorods shown in Fig. 1a and $w_{Si-Cu} = 220 \pm 50$ nm for Si–Cu nanorods shown in Fig. 1c. From the cross-section view images, the thickness and length of the nanorods are $d_{Si} = 90 \pm 30$ nm and $l_{Si} = 4\,\mu$m (Fig. 1b), and $d_{Si-Cu} = 60 \pm 20$ nm and $l_{Si-Cu} = 2.7\,\mu$m (Fig. 1d), respectively. In addition, a layer of ~ 200 nm thick Cu film is visible between the nanorods and the substrate for both the samples (Fig. 1b and d).

To obtain the crystal structure, both the Si and Si–Cu nanorods were deposited directly on glass substrates for XRD characterization. The obtained XRD patterns are displayed in Fig. 2. The XRD results show that the as-deposited Si nanorods are amorphous (Fig. 2a); however, when co-deposited with Cu, a polycrystalline orthorhombic Cu_3Si phase forms, as revealed by the peak Cu_3Si

(0 1 2) at $2\theta \approx 44.57°$ in Fig. 2b. By applying the Scherrer formula [18] to this peak, the average Cu_3Si crystal size is estimated to be $D_{Cu_3Si} \approx 2.4$ nm in diameter, which can be further confirmed by the TEM images in Fig. 3. In the TEM images, the light part is amorphous Si matrix and the dark parts are Cu_3Si nanoparticles with the size of $D_{Cu_3Si} = 2.4 \pm 0.6$ nm, which is consistent with that obtained from the XRD analysis. Therefore, the Si–Cu nanorods are composed of the polycrystalline Cu_3Si nanoparticles embedded in the amorphous Si nanorod matrix.

The force–displacement curves of Si and Si–Cu nanorods are plotted in Fig. 4. The color variation represents different nanorods
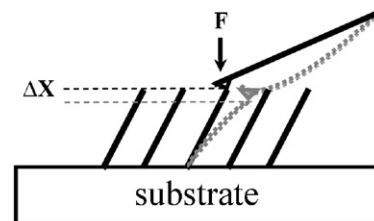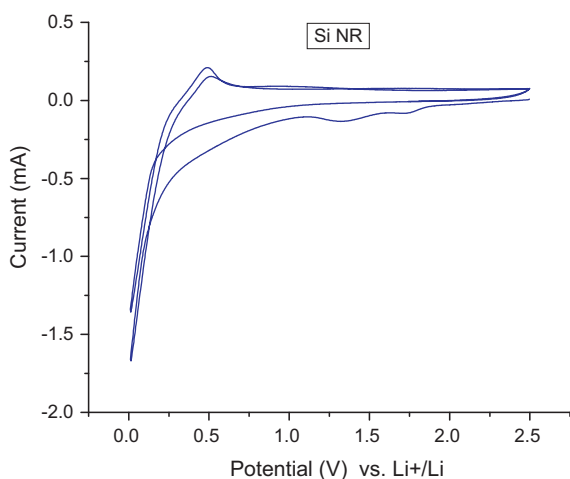

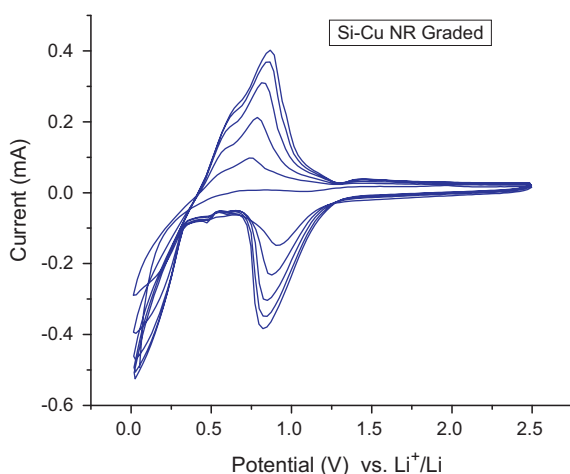(a) The schematic of the measurement of the force-displacement
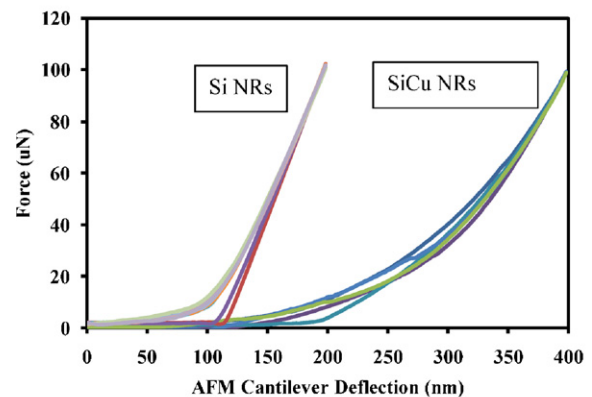
(b) The result of force-displacement curves under same force

Fig. 4. The measurement of the force–displacement of the Si nanorods and Si–Cu nanorods.
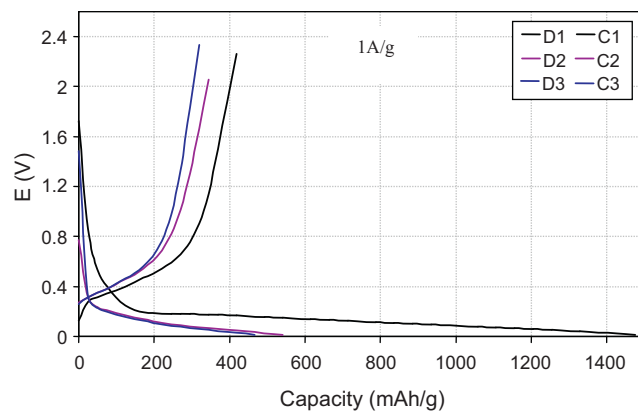
(a) CV of Li/Si cell (2 cycles)

(a) The first three cycles of Li/Si NR cell
(Note: D1-first discharge, C1-first charge)

(b) CV of Li/SiCu cell (5 cycles)

Fig. 5. The cyclic voltammograms (CV) of Li/Si and Li/Si–Cu cells.

(b) The cyclability of Li/Si NR cell

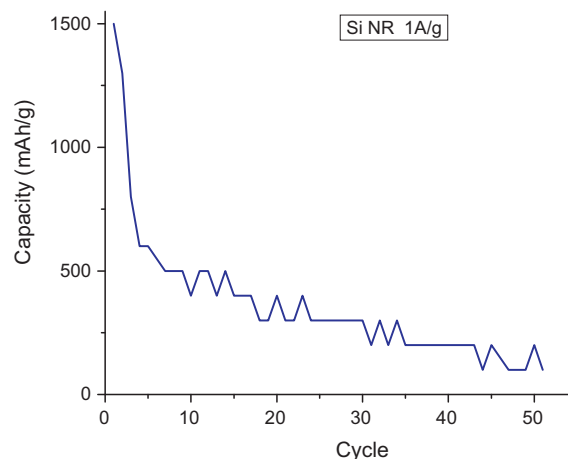**Fig. 6.** The cycling performance of the Li/Si NR cell.

that were tested. As seen, the force–displacement measurements are quite consistent indicating that the fabricated nanorods have uniform structural quality and statistical errors are minimal. One should note that the slope of load–displacement curves in Si–Cu NRs ($\theta_{SiCu\ NR}$) is considerably lower than the ones in Si nanorods ($\theta_{Si\ NR}$), which indicates that the Si–Cu nanorods are more flexible than the Si nanorods.

2.2. Cyclic voltammograms of the Si and Si–Cu nanorods

The cyclic voltammograms (CV) of Li/Si and Li/Si–Cu cells are shown in Fig. 5. In the first cathodic scan (charging) of the Li/Si NR cells, the current increase at 1.70 V and 1.35 V may correspond to reduction of silicon oxide covering out layer of the Si nanorods that disappeared in the following cycles. The large current increase at 0.3 V was resulted by formation of Li–Si alloy. According to the reported data [19], the corresponding Li–Si alloy could be $Li_{13}Si_4$. There are four confirmed Li–Si alloy phases: $Li_{12}Si_7$, Li_7Si_3, $Li_{13}Si_4$ and $Li_{22}Si_5$. The lithiation process can be illustrated as: $xLi^+ + ySi + xe^- \rightarrow Li_xSi_y$ ($x = 12, 7, 13, 21, y = 7, 3, 4, 5$). In the anodic scan, the reduction peak at 0.5 V that may correspond to delithiation of $Li_{13}Si_4 \rightarrow 11Li + 2LiSi_2$. The Li/Si–Cu NR cells show a different electrochemical behavior. Li does not form alloys with Cu and has 3% of solubility in Cu. However, co-depositing Cu in Si changes the

feature of CV. The large current peak at 0.83 V in cathodic scan cannot be interpreted yet. It is speculated that the peak may correspond to solution of Li in Cu. The second current increase at ~0.25 V corresponds to Si lithiation. The shift of peak position may be caused by the addition of Cu. In anodic scan, the first peak at 0.62 V may correspond to delithiation of Li–Si alloy. The second peak at 0.88 V may relate to dissolution of Li from Cu.

2.3. The cyclability and morphology changes of Si nanorods and Si–Cu nanorods

The Li/Si nanorod cell demonstrated the capacity of 1500 mAh g^{-1} in the first discharge cycle (Fig. 6a). However, the high capacity was quickly diminished in the following 50 cycles (Fig. 6b). It is likely that the high surface area of Si nanorods may be covered by SiO_2 formed during samples transfer in the ambient air. Some of Li was consumed to reduce SiO_2 in the first discharge (Li insertion), which is thermodynamically favorable. The Li ion conductivity of Li_2O is higher than SiO_2. The dipping of the potential at 1.5 V may indicate the completion of SiO_2 reduction and Li_2O formation as discussed in Fig. 5c. It is believed that the pallation of the brittle Si nanorods (Li loss) and the detachment of the Si nanorods from current collector (poor electronic conductivity) lead to the sloped discharge curve and diminishing capacity. The SEM images shown in Fig. 7 indicate that the Si nanorods are expanded when charged to 1.2 V (~50% capacity)

(a) Virgin Si NR

(b) 50% discharged Si NR in the first cycle

(c) 100% discharged Si NR in the first cycle

(d) 100% discharged Si NR after 100 cycles

(e) TEM images of the charged Si NR (new lattice and strain introduced)

(f) TEM images of the discharged Si NR (in amorphous state)
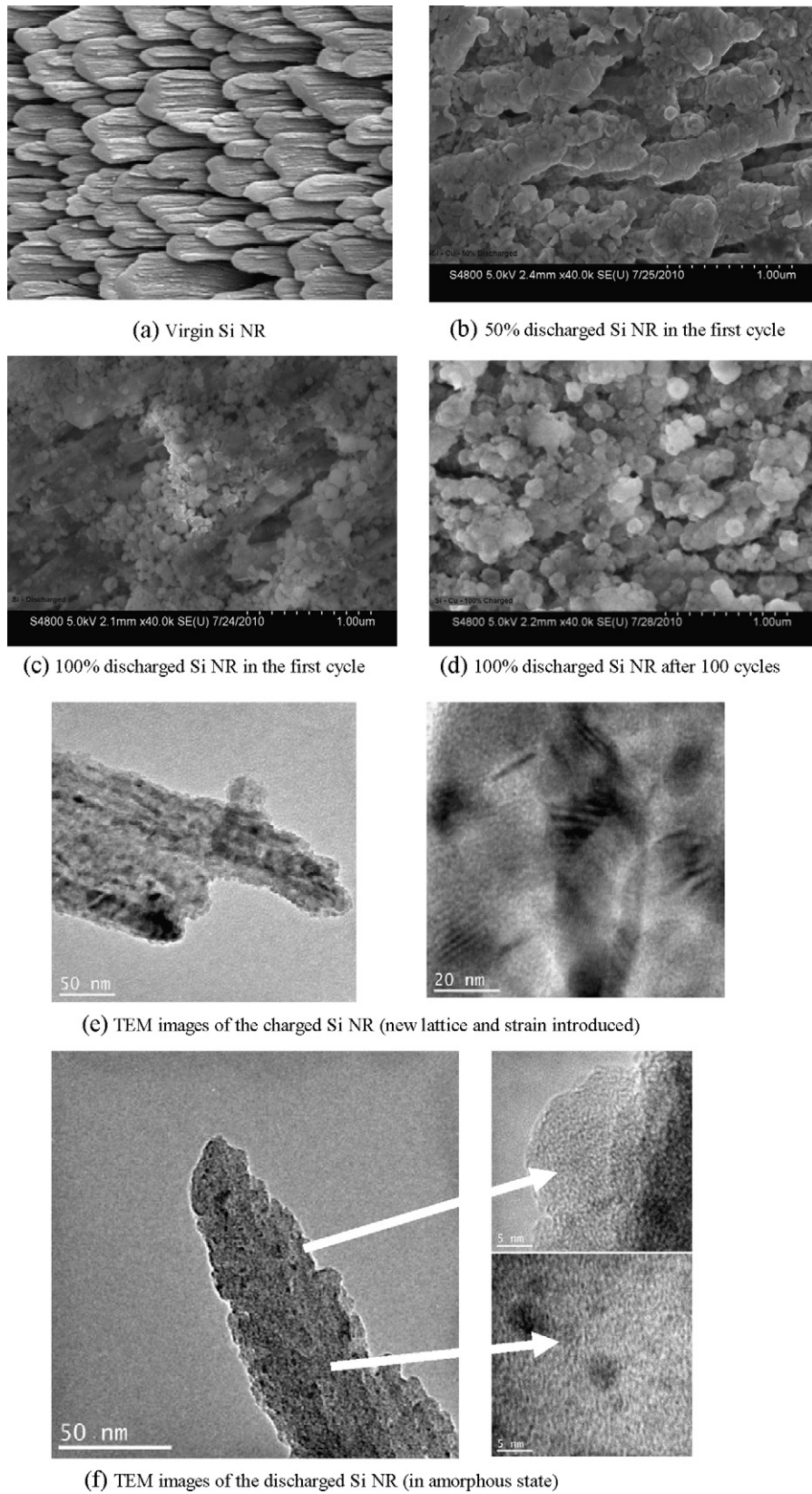
Fig. 7. The morphology changes of Si NR after charged.

and pulverized when the anode is charged continuously to 2.4 V (~100% capacity). The alignment in the as-deposited Si nanorods is also destroyed when the Si nanorod anode is charged to 50% capacity. The top view SEM image (Fig. 7b) shows nanorods with an

enlarged diameter. When the anode is charged to 100% capacity, as shown in Fig. 7c, the original nanorods became nanoparticles, and one can hardly recognize any nanorod remained on the substrate. After 100 cycles, the Si nanorods become loose particles and
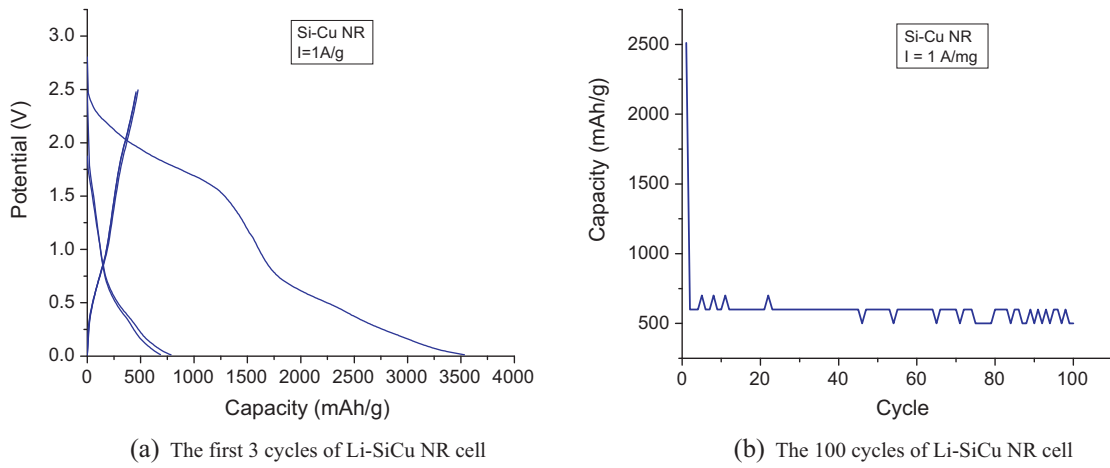
(a) The first 3 cycles of Li-SiCu NR cell

(b) The 100 cycles of Li-SiCu NR cell

Fig. 8. The cycling performance of the Li/SiCu NR cell.

(a) The virgin Si-Cu NR

(b) The full discharged Si-Cu NR in the first cycle still shows the nanorod structure

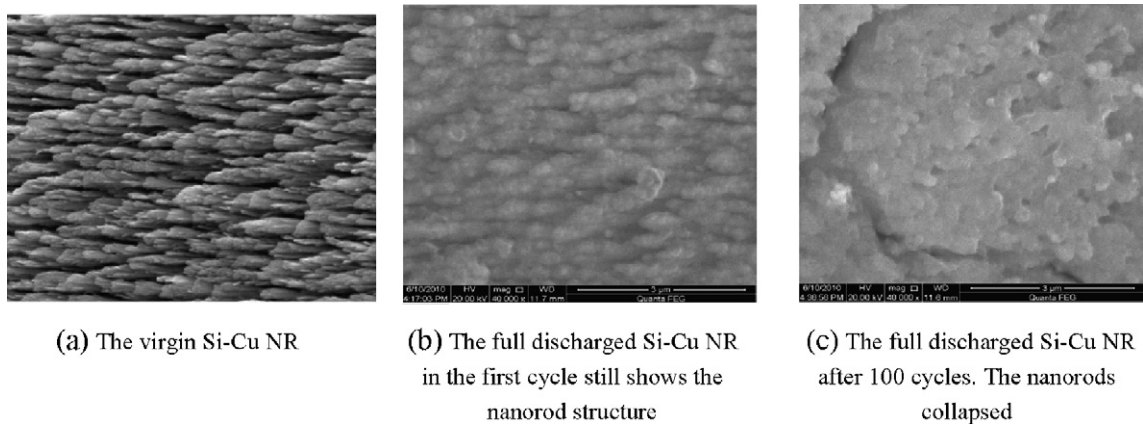(c) The full discharged Si-Cu NR after 100 cycles. The nanorods collapsed

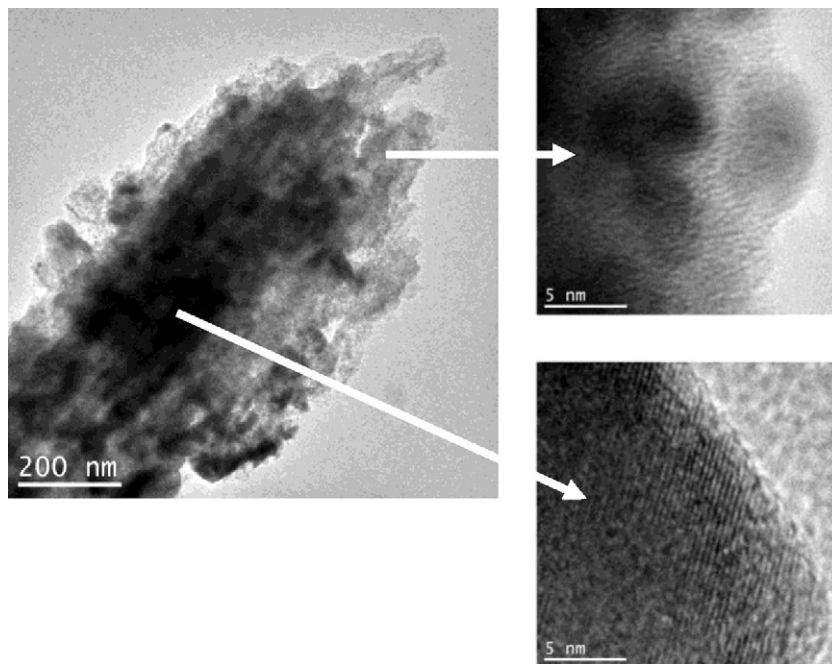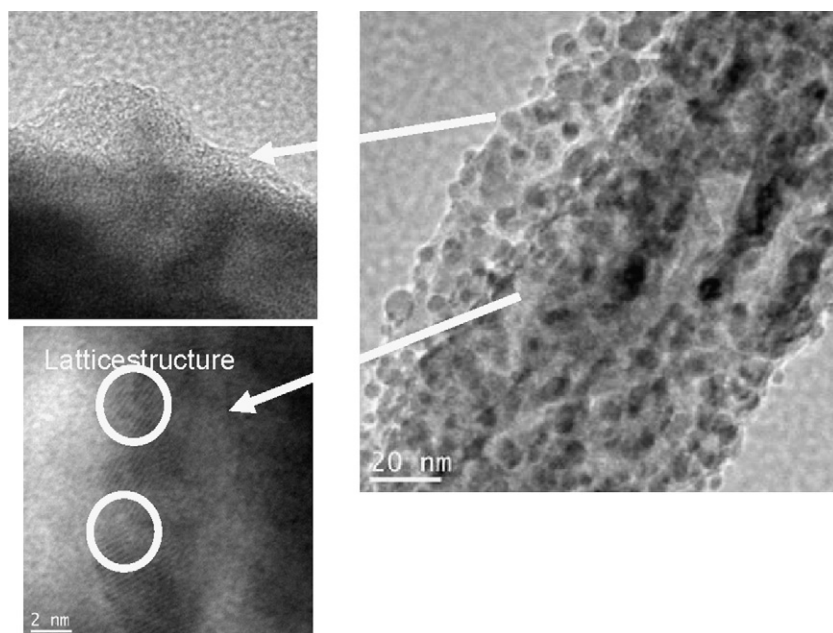**Fig. 9.** The morphology changes of the Si–Cu nanorods.

Fig. 10. TEM image of the virgin Si–Cu NR shows the amorphous structure with scattering crystalline regions corresponding to Si–Cu compounds.
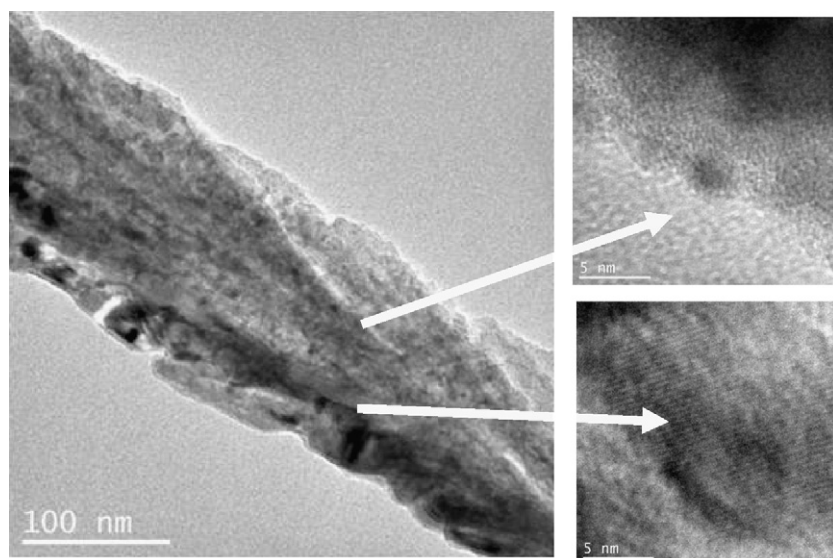
Fig. 11. TEM images of the charged SiCu NR shows the rough surface and amorphous-crystalline mixed structure. The crystalline regions correspond to the Si–Cu compounds.

lose direct electrical contact with the Cu substrate, resulting in diminishing of the storage capacity (Fig. 6a). The TEM images show that the lithiation introduces crystallization of Li–Si compounds (new lattice pattern) companioning with the fringes generated by local stain and stress (Fig. 7e). After delithiation, the nanorods return to amorphous state with rough surface (Fig. 7f).

The Li/Si–Cu nanorod cell performs differently. It demonstrated 3500 mAh g^{-1} capacity in the first discharge (Fig. 8a). The higher initial discharge capacity of Si–Cu nanorods anode may attribute to its high electronic conductivity by adding Cu. The capacity decreased to 800 mAh g^{-1} in the second cycle, but sustainable at 500 mAh g^{-1} in following 100 cycles (Fig. 8b). Several facts could be responsible for the irreversible capacity loss in the first cycle (2700 mAh g^{-1}): (1) the formation of solid electrochemical interface (SEI) that consumes Li and increases the anode impendence; (2) the reduction of SiO$_2$ causing permanent loss of Li and (3) the crystallization of the amorphous Si–Cu matrix during the first discharge generates locals stress and strain that may hinder Li ion insertion process.

The SEM observation shows that the surface of Si–Cu nanorods become rough, but the structures remain in aligned orientation after full discharged (Fig. 9). Due to its mechanical flexibility and less brittle nature (see Fig. 4), the Si–Cu nanorods are able to maintain better integrity compared to Si nanorods and can survive for 100 cycles. The TEM shows the virgin Si–Cu nanorods have the amorphous and crystalline mixing structure. The crystalline regions correspond to Si–Cu compounds such as Cu$_3$Si and Cu$_5$Si (Fig. 10). Similar as the Si NR, the lithiation of Si–Cu NR produces Li–Si alloys through the phase transformation process introducing strain and stress that causes surface roughness (Fig. 11). After discharge, most Li left the anode and the surface of Si–Cu NR returns to smooth, but the crystalline grains (thermodynamic stable) and non-relaxed strain remained in SiCu matrix. The local stress does not seem relaxed completely (Fig. 12). It implies that the changes

Fig. 12. TEM images of the discharged SiCu NR shows the smooth surface, amorphous and crystalline regions mixed structure.

of the morphology and amorphous-crystalline structural change of Si nanorods and Si–Cu nanorods are partially reversible due to the metastable nature of the amorphous structure. Si and Si–Cu anodes do not form the solid electrochemical interface (SEI) as the carbon anodes do. The large capacity lose in the first cycle may relate to partially irreversible structure and morphology changes. It is found that the cyclable capacity can be sustained by adding of Cu in the nanostructured Si anodes.

3. Conclusions

The aligned Si nanorods show anodic capacity of 1500 mAh g^{-1} during the first charge–discharge cycle. The high initial capacity decreases rapidly and becomes diminished after 50 discharge–charge cycles. This behavior is attributed to the serve morphology change and pulverization due to the brittle nature of the silicon. Si–Cu composite nanorods demonstrates 3500 mAh g^{-1} capacity in the first charge–discharge cycle. Although the capacity is in fact decreased to 800 mAh g^{-1} in the second cycle, it is sustainable at 500 mAh g^{-1} for 100 cycles. SEM, TEM and AFM analyses indicate that adding Cu into the Si nanorods provides the mechanical flexibility and reduces the brittleness of silicon, thus makes the structure more stable. The morphology change of Si and Si–Cu nanorods during electrochemical charge and discharge are partially reversible and may contribute to low columbic effect and unrecoverable capacity loss in the first cycle. Tuning the composition and the structure of nanostructured Si will lead to practical approach to leverage the advantage of Si based anode materials in Li-ion battery application.

Acknowledgements

References

[1] M. Au, S. McWhorter, H. Ajo, T. Adams, Y.P. Zhao, J. Gibbs, J. Power Sources 195 (2010) 3333–3337.
[2] M. Green, E. Fielder, B. Scrosati, M. Wachtler, J.S. Moreno, Electrochem. Solid State Lett. 6 (5) (2003) A75–A793.
[3] E. Hosono, H. Matsuda, I. Honma, M. Ichihara, H.S. Zhou, J. Electrochem. Soc. 154 (2007) A146–A149.
[4] M.D. Fleischauer, M.N. Obrovac, J.R. Dahn, J. Electrochem. Soc. 155 (2008) A851–A854.
[5] R.Z. Hu, M.Q. Zeng, C.Y.V. Li, M. Zhu, J. Power Sources 188 (2009) 268–273.
[6] X.F. Lei, C.W. Wang, Z.H. Yi, Y.G. Liang, J.T. Sun, J. Alloys Compd. 429 (2007) 311–315.
[7] C.K. Chan, X.F. Zhang, Y. Cui, Nano Lett. 8 (2008) 307–309.
[8] C. Villevieille, C.M. Ionica-Bousquet, B. Ducourant, J.C. Jumas, L. Monconduit, J. Power Sources 172 (2007) 388–394.
[9] A. Caballero, J. Morales, L. Sanchez, J. Power Sources 175 (2008) 553–557.
[10] C. Liu, F. Li, L.P. Ma, H.M. Cheng, Adv. Mater. 22 (2010) E28.
[11] M. Au, T. Adams, J. Mater. Res. 25 (2010) 1649–1655.
[12] C. Chan, H. Peng, G. Liu, K. McIlwrath, X.F. Zhang, R. Huggins, Y. Cui, Nat. Nanotechnol. 3 (2008) 31–35.
[13] R. Krishnan, T.-M. Lu, N. Koratkar, Nano Lett. 11 (2011) 377–384.
[14] Y.P. He, Z.Y. Zhang, C. Hoffmann, Y.P. Zhao, Adv. Funct. Mater. 18 (2008) 1676–1684.
[15] Y.P. He, Y.P. Zhao, J.S. Wu, Appl. Phys. Lett. 92 (2008).
[16] Y.P. He, J.G. Fan, Y.P. Zhao, Int. J. Hydrogen Energy 35 (2010) 4162–4170.
[17] Y.P. He, J.G. Fan, Y.P. Zhao, Cryst. Growth Des. 10 (2010) 4954–4958.
[18] A.L. Patterson, Phys. Rev. 56 (1939) 978–982.
[19] W.J. Weydanz, M. Wohlfahrt-Mehrens, R.A. Huggis, J. Power Sources 81–82 (1999) 237–242.